



Analysis of Antarctic ozone trends from 1979 to 2023

Haotian He¹, Martyn P. Chipperfield^{2,3}, Sandip S. Dhomse^{2,3}, Wuhu Feng^{2,4}, Shujie Chang^{1,2}, Yajuan Li^{5,6}, Mark Weber⁷ and Saffron Heddell²

¹College of Ocean and Meteorology, South China Sea Institute of Marine Meteorology, Laboratory for Coastal Ocean
5 Variation and Disaster Prediction, Key Laboratory of Climate Resources and Environment in Continental Shelf Sea and
Deep Ocean (LCRE), Key Laboratory of Space Ocean Remote Sensing and Application, Ministry of Natural Resources,
Guangdong Ocean University, Zhanjiang, China

²School of Earth and Environment, University of Leeds, Leeds, UK

³National Centre for Earth Observation (NCEO), University of Leeds, Leeds, UK

10 ⁴National Centre for Atmospheric Science (NCAS), University of Leeds, Leeds, UK

⁵School of Electronic Engineering, Nanjing Xiaozhuang University, Nanjing, China

⁶Key Laboratory of Middle Atmosphere and Global Environment Observation, Institute of Atmospheric Physics, Chinese
Academy of Sciences, Beijing, China

⁷Institute of Environmental Physics, University of Bremen, Bremen, Germany

15 *Correspondence to:* Shujie Chang (changsj@gdou.edu.cn)

Abstract. Antarctic ozone has shown a sustained recovery since 2000, but levels were distinctly low during 2020-2023,
potentially affecting estimates of ozone recovery and long-term trends. To assess the impact of recent low ozone on long-
term variability, we analyze total column ozone (TCO) data from World Ozone and Ultraviolet Radiation Centre, multi-
20 sensor reanalysis, and Total Ozone Mapping Spectrometer/Ozone Monitoring Instrument. Ozone fields from TOMCAT, a 3-
D chemical transport model, are also used to gain better insight ozone changes. Multiple linear regression (MLR) is applied
to estimate ozone trends over Antarctica from 1979 to 2023, incorporating proxies representing key chemical and dynamical
processes such as the El Niño-Southern Oscillation and the Brewer-Dobson circulation (BDC).

25 Our analysis suggests that before 2000, all datasets show significant declines in annual TCO of about 2 and 6 Dobson Units
per year (DU/yr) for September and October, respectively. For the 2001-2023 period, the magnitude of the October trend
shifted to -1.5 DU/yr. The MLR effectively captures long-term ozone changes as well as unusual dynamical events such as
the sudden stratospheric warmings in 2002 and 2019. As dynamical proxies show the largest influence, we use TOMCAT
30 simulations to illustrate the impact of the BDC on the Antarctic ozone. Two sensitivity simulations further demonstrate that
the strengthening (weakening) of the circulation leads to high (low) ozone values in spring. These findings suggest that after



ozone-depleting substances were strictly controlled, dynamical processes have played an increasingly important role in controlling the ozone recovery patterns in Antarctica.

1 Introduction

35 The discovery of the Antarctic ozone hole in 1985 sparked decades of intensive research on the causes of stratospheric ozone depletion and its broader climate implications (Farman et al., 1985; Solomon et al., 1986). Early scientific studies correctly established link between the decline in the Antarctic ozone and anthropogenic emissions of halogenated ozone-depleting substances, such as trichlorofluoromethane (CFC-11) and dichlorodifluoromethane (CFC-12) (e.g. WMO, 2014, 2018, 2022). These compounds historically contributed to a large portion of the stratospheric chlorine loading. In response to this environmental threat, the 1987 Montreal Protocol and its subsequent amendments were successfully implemented which led to reduction in stratospheric chlorine and bromine loading (WMO, 2022). Beyond their role in ozone depletion, these halogenated substances are also potent greenhouse gases with high global warming potentials, meaning their phase-out has provided substantial co-benefits for climate change mitigation (e.g. Ramanathan et al., 1985; Velders et al., 2007).

45 These regulatory measures led to stabilising in global ozone trends and initiated a gradual recovery toward pre-1980 conditions (e.g. Dhomse et al., 2018; WMO, 2022). Significant signs of recovery have been confirmed in the upper stratosphere, where ozone increases are attributed to both declining halogens and stratospheric cooling resulting from increased greenhouse gas abundances (Chipperfield et al., 2017; Steinbrecht et al., 2017; Godin-Beekmann et al., 2022). However, the evolution of the lower stratosphere remains a subject of ongoing debate and high uncertainty (Chipperfield et al., 2018). Several observation-based studies suggest a continued decline in lower-stratospheric ozone since 1998, which has been linked to changes in stratospheric dynamics and increased tropical upwelling (Ball et al., 2018; Wargan et al., 2018). In the Antarctic region specifically, while a sustained recovery has been observed since 2000, the period between 2020 and 2023 was characterized by exceptionally large and long-lasting ozone holes (Kessenich et al., 2023). The accurate quantification of how these recent perturbations affect long-term recovery trends remains unclear.

55 Antarctic ozone variability depends not only on declining halogens but also on a complex interplay of chemical and dynamical processes that vary across multiple timescales. External climate forcing, such as 11-year solar variability and sporadic volcanic eruptions, exerts a significant influence on polar ozone levels (Dhomse et al., 2016, 2022). Increased ultraviolet radiation during solar maxima enhances ozone production in the upper stratosphere (Gray et al., 2010). Major volcanic events, such as Mount Pinatubo in 1991, have caused significant mid-latitude ozone depletion through heterogeneous chemical processing on sulphate aerosols (Aquila et al., 2013; Dhomse et al., 2015). More recently, the 2022 eruption of the Hunga Tonga-Hunga Ha'apai volcano and major wildfires, such as the 2019-2020 Australian fires, have been

identified as significant perturbations that altered stratospheric aerosol loading and water vapor, potentially delaying the expected recovery of the ozone hole (Khaykin et al., 2020; Peterson et al., 2021; Zhou et al., 2024).

65

The use of multiple linear regression (MLR) has greatly improved our understanding of these chemical and dynamical processes by allowing for the assessment of various proxies on ozone variability (Dhomse et al., 2006; Steinbrecht et al., 2017; Ball et al., 2019; Weber et al., 2022; Li et al., 2023). Key proxies utilised in such analyses include the quasi-biennial oscillation, El Niño-Southern Oscillation, and the Antarctic Oscillation (Chehade et al., 2014; Weber et al., 2018).

70

Dynamical processes, particularly the Brewer-Dobson circulation, exert a dominant influence on the seasonal and interannual variability of Antarctic ozone (Weber et al., 2011; Butchart, 2014). As ozone-depleting substances are strictly controlled, the relative importance of these dynamical drivers in determining the recovery pattern has increased (Li et al., 2023). However, regression models can be prone to overfitting due to the complex coupling and correlation between different atmospheric proxies (Dhomse et al., 2022; Li et al., 2023).

75

The aim of this paper is to assess the latest long-term trends of total column ozone over Antarctica using updated observational data from the World Ozone and Ultraviolet Radiation Data Centre, multi-sensor reanalysis fields, and 3-D chemical transport model simulations up to the end of 2023. Given that Antarctic depletion is most pronounced during the Southern Hemisphere Spring, we focus on spring ozone changes to quantify the contributions of key factors to ozone variability. The structure of this manuscript is as follows: Section 2 introduces the ozone datasets and the TOMCAT model configuration, followed by MLR methodology in Sect. 3. Section 4 presents analyse long-term trends and proxy contributions, and Section 5 discusses the results of model sensitivity experiments, followed by a summary and conclusions (Section 6).

85 **2 Ozone datasets**

TCO data from the World Ozone and Ultraviolet Radiation Data Centre (WOUDC), the Multi-sensor reanalysis (MSR-2) and Total Ozone Mapping Spectrometer/Ozone Monitoring Instrument (TOMS/OMI) are utilised in this study to assess long-term Antarctic variations. In addition to these observational products, ozone profile datasets simulated by the global three-dimensional chemical transport model, TOMCAT, is also used to provide consistency for the analysis and to gain better insight into vertical changes. A detailed summary of the data sources and their respective spatio-temporal resolution are shown in Table 1.

90



2.1 WOUDC data

The WOUDC ground-based dataset is generated by merging measurements from Dobson and Brewer spectrophotometers along with filtered ozonometers. Zonal mean ozone value is derived using the method of calculating the "climatological" ozone deviation of stations, followed by smoothing or approximation across different stations and months to reduce uncertainty, resulting in 5° zonal averages (Fioletov et al., 2002). To ensure high data quality, the WOUDC records undergo rigorous filtering to eliminate systematic errors or unreliable results. These ground-based observations typically show excellent agreement with satellite-derived data, usually within $\pm 0.5\%$, ensuring high consistency between the merged satellite records and the ground-based observations utilised here (Chiou et al., 2014).

100 2.2 MSR data

The MSR dataset is a comprehensive, revised ozone product constructed by merging measurements from 14 different satellite retrieval instruments. These include the TOMS series (Nimbus-7 and Earth Probe), SBUV (Nimbus-7, NOAA-9, NOAA-11 and NOAA-16), GOME (ERS-2), SCIAMACHY (Envisat), OMI (EOS-Aura), and GOME-2 (Metop-A). Systematic biases in all satellite records are first corrected using independent ground-based total ozone data from the WOUDC, accounting for factors such as solar zenith angle, viewing angle, trend, and effective ozone temperature. The final global ozone dataset is generated using data assimilation techniques based on a chemical transport model driven by meteorological fields from the European Centre for Medium-Range Weather Forecasts (ECMWF) (Van Der A et al., 2010).

2.3 TOMS/OMI data

TOMS continuously measures the sunlit regions of the Earth. The Version 8 total ozone column measurements from TOMS onboard Earth probe (TOMS-EP) were used in this study (Wellemeier et al., 2004). OMI, onboard the Aura satellite, continues to monitor ozone columns in the atmosphere as a continuation of the TOMS series. OMI measurements provide extremely high spatial resolution and have made significant contributions to the study of stratospheric and tropospheric chemistry (Levelt et al., 2006, 2018).

2.4 TOMCAT model data

115 TOMCAT is a three-dimensional chemical transport model (CTM) that simulates global data for stratospheric chemical elements and substances such as ozone based on consistent chemical equations (Chipperfield, 2006). The model includes a comprehensive chemical scheme and is driven by ERA-5 reanalysis meteorological fields provided by the ECMWF. Model setup is similar to the one used in Zhou et al. (2024). Time varying solar spectral irradiances are from NRL v2 (Coddington et al., 2016) that are extended until December 2023. Variations in stratospheric aerosol resulting from volcanic eruptions are represented by stratospheric sulphate area density (SAD) fields. These fields are same as used in CMIP6 simulations (until 120 December 2016) and for later period, we use SAGE III measurements based SAD data products (Knepp et al., 2024).



Implementation of SAD and solar spectral irradiance (SSI) variations is described by Dhomse et al. (2015, 2016). TCO values from the model are calculated by vertical integration of these simulated ozone profiles.

125 Table 1. Sources and temporal coverage of ozone datasets.

Dataset	Start and end year	Spatio-temporal resolution	Source
WOUDC	1979-2023	Monthly; 5° zonal mean of TCO	http://woudc.org/archive/Projects-Campaigns/ZonalMeans
MSR-2	1979-2023	Monthly; lat * lon = 360 * 720 with TCO	https://www.temis.nl/protocols/O3global.php
TOMS/OMI	2001-2023	Monthly; lat * lon = 180 * 360 with TCO	https://disc.gsfc.nasa.gov/datasets/TOMSEPL3mt_oz_008 and https://www.earthdata.nasa.gov/learn/find-data/near-real-time/omi
TOMCAT	1979-2023	Daily; T42 L32	Simulation of Global Ozone Data based on EAR 5 (Chipperfield, 2006).

3 Methods

3.1 Multiple linear regression (MLR)

Ozone trends are generally estimated using MLR, which uses linear trend terms to quantify long term changes due to unknown processes and also includes proxies for the known dynamical and chemical processes. Various methods have been applied to represent trend terms in MLR, such as the piecewise linear trends (PLT), the independent linear trends (ILT), and the equivalent effective stratospheric chlorine (EESC) to account for long term ozone changes due to changes in the ODS (Harris et al., 2008; Nair et al., 2013; Chegade et al., 2014). These trend terms represent the only non-periodic terms of MLR, and aside from ODS, any aperiodic term for ozone change is attributed to this trend term. Previous studies show that stratospheric cooling, due to increases in greenhouse gases, and ODS have comparable effects on ozone increase, while EESC only reflects the chemical influence of ODS. Not all aperiodic changes can be assumed to follow EESC, hence we employ ILT as the trend term of the MLR and ILT and all proxies match the entire period. Using factors such as QBO, 11-

year solar cycle, ENSO, Antarctic Oscillation (AAO), BDC, stratospheric aerosol optical depth (AOD) (Weber et al., 2018, 2022), the MLR equation used here is shown in Eq. (1):

140

$$y(t) = a_1 \cdot X_1(t_1) + a_2 \cdot X_2(t_2) + \alpha_{QBO10} \cdot QBO_{10}(t) + \alpha_{QBO30} \cdot QBO_{30}(t) + \alpha_{AOD} \cdot AOD(t) + \alpha_{sun} \cdot S(t) + \alpha_{BDC} \cdot BDC(t) + \alpha_{ENSO} \cdot E(t) + \alpha_{AAO} \cdot AAO(t) \quad (1)$$

145

where $y(t)$ is the ozone time series, with t representing the year of the observation, a_1 and a_2 are the linear trend before and after EESC reaches maximum over the Antarctic. t_1 and t_2 indicate that X_1 and X_2 are only different from zero for years t before (1979-2000) and after (2001-2023) the EESC peak, respectively. Analysis of ozone data shows a turning point in the continued decline of Antarctic ozone around 2000, consistent with the EESC calculations showing a maximum in the polar regions at that time (Newman et al., 2006, 2007).

3.2 Proxy for main impact factors

150

Sources of proxy data are shown in Table 2. To account for the effect of QBO phases and strength on ozone, equatorial zonal winds (10 hPa and 30 hPa) are commonly utilized as indices (Chehade et al., 2014; Li et al., 2020). AOD has been used to represent volcanic aerosol changes following eruptions such as those of El Chichón and Pinatubo volcanoes, which have been shown to affect ozone in the Southern Hemisphere (Sato et al., 1993; Aquila et al., 2013; Dhomse et al., 2015). The AOD proxies are provided as a function of latitude, while we utilised the SH average aerosol data. To account for solar variability, a driver of long-term ozone changes, we use Bremen composite Mg II index (Snow et al., 2014). The BDC is usually expressed as the eddy heat flux (EHF) at 100 hPa, a proxy widely used to access dynamical influence on the interannual ozone variability (e.g. Newman et al., 2001; Dhomse et al., 2006; Weber et al., 2011). ENSO variability is also known to have significant impact on the Southern Hemisphere stratosphere, leading to early or delayed break-up of the polar vortex (e.g. Randel et al., 2002; Camp and Tung, 2007). AAO is closely related to the Antarctic ozone hole (Thompson and Solomon, 2002). Thus, AAO and ENSO are included as proxies for long-term ozone change. In the MLR, AAO and EHF are represented by the mean of the autumn-to-spring accumulation, while other proxies use the monthly mean time series.

160

Table 2. Sources of impact proxies.

Proxy	Explanatory proxy	url / file
QBO 10 hPa, QBO 30 hPa	Singapore wind speed at 30 hPa and 10 hPa	https://www.iup.uni-bremen.de/OREGANO/proxy/qbo_era5_6S-6N_zonalwind_monthly_mean_1979-2024.txt
AOD(t)	Stratospheric aerosol optical depth at	https://asdc.larc.nasa.gov/project/GloSSAC



550 nm

S(t)	Bremen composite Mg II index	https://www.iup.uni-bremen.de/UVSAT/data/
BDC(t)	Eddy heat flux (100 hPa, 45 S°-75 S°)	https://www.iup.uni-bremen.de/OREGANO/proxy/chf_m_era5_100hPa_accumulated.txt
E(t)	Multivariate ENSO Index (MEI V2)	https://psl.noaa.gov/data/climateindices/list/
AAO(t)	Antarctic Oscillation (AAO)	https://www.cpc.ncep.noaa.gov/products/precip/CWlink/daily_ao_index/aao/aao.shtml

165 An important criterion of MLR is that the impact proxies should not be highly correlated with each other. As shown in Fig. 1, correlations among the proxies are minimal, with the highest coefficient at 0.3, satisfying the precondition for MLR analysis. Therefore, these proxies are suitable for analyzing long-term ozone changes.

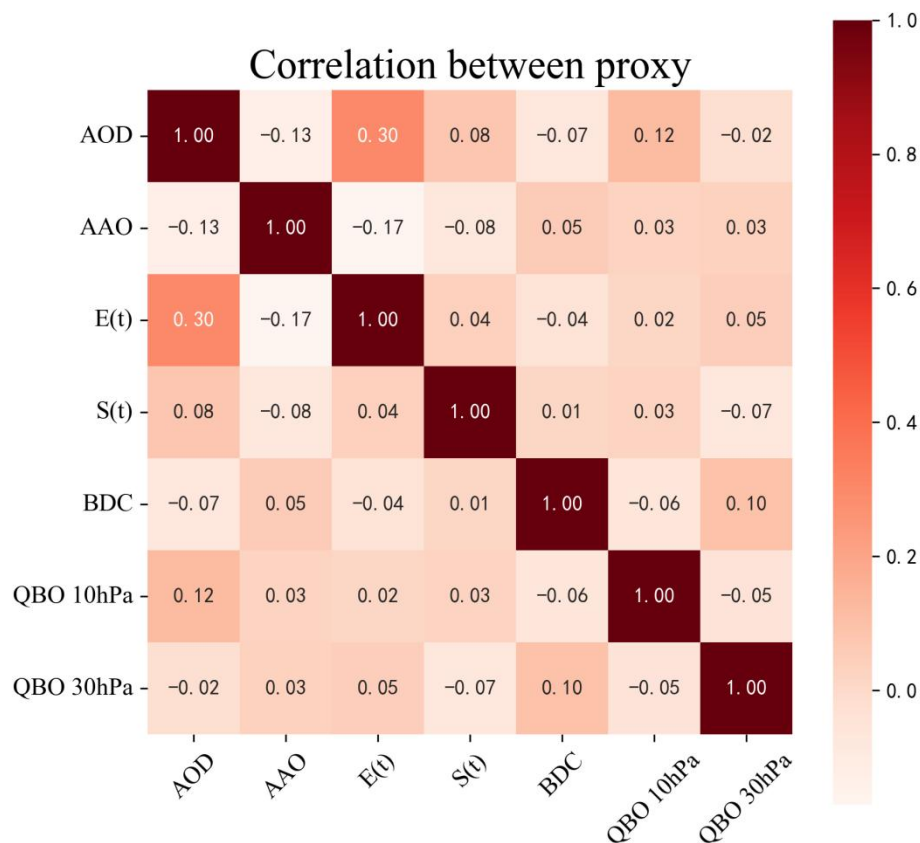


Figure 1. Correlation coefficients among the main impact proxies.

170

4 Long-term trends in Antarctic ozone

Antarctic ozone recovery exhibits strong seasonal dependence, particularly the contrasting behavior in September and October. Figure 2 illustrates the long-term ozone trends in the Antarctic region (60°S-90°S) from four datasets, reflecting the persistence of the deep ozone hole and extended periods of low ozone over Antarctica in recent years. Among these, WOUDC data indicate relatively small fluctuations in TCO values. In contrast, the TOMCAT and MSR2 exhibit more pronounced variations. To ensure consistency across datasets with different temporal coverage, trends were analyzed for 2001- 2023. During this period, September shows signs of recovery, whereas October exhibits a notable decline of approximately -1 DU/yr. Overall, the ozone variations among the datasets show good consistency, and we examined trends across different time spans to clarify these seasonal behaviors.

180

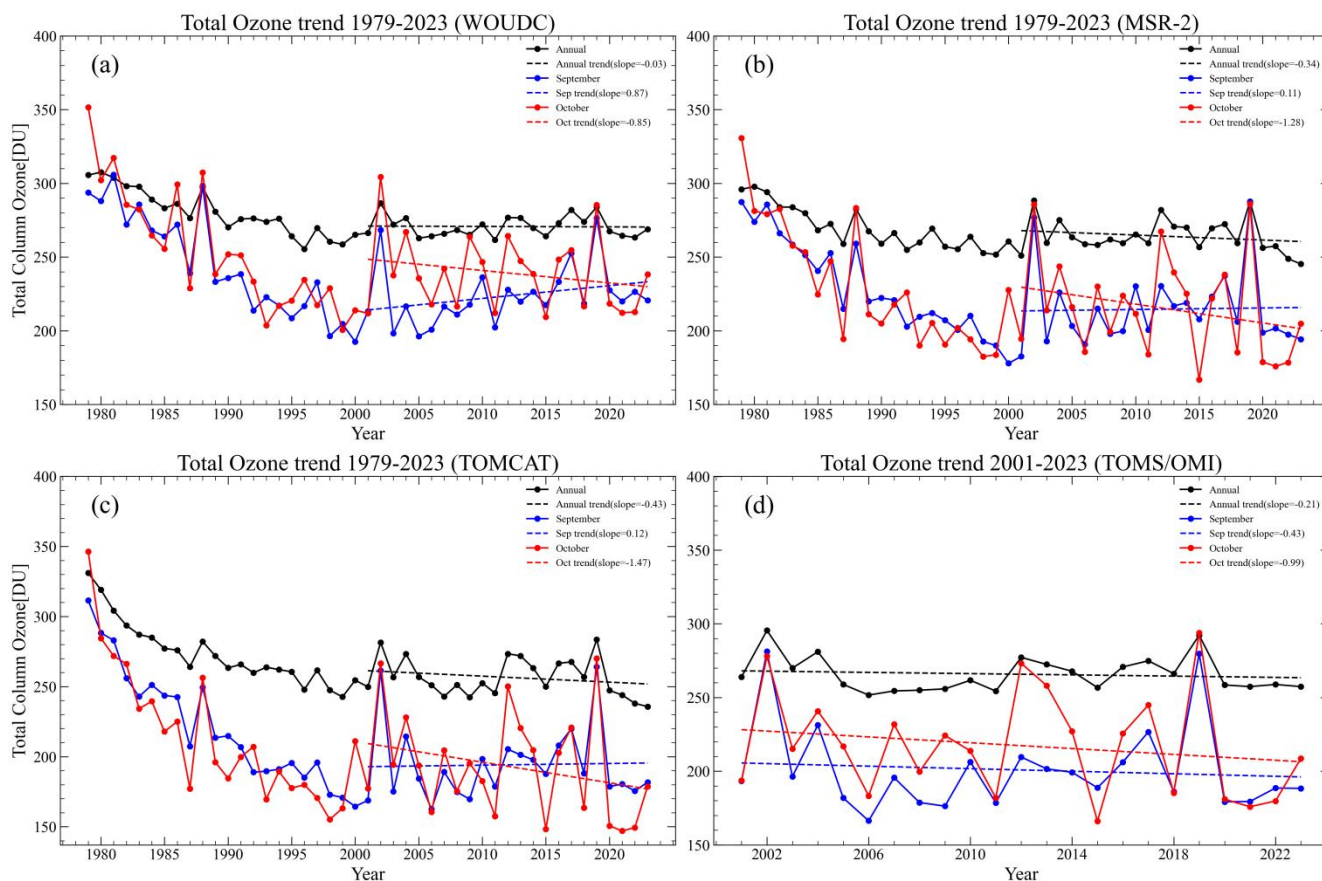


Figure 2. The TCO time series in the Antarctic (90°-60°S) from multiple datasets. (a) WOUDC, (b) MSR, (c) TOMCAT, and (d) TOMS/OMI. The black line represents the annual mean time series, the blue line represents the September time series, and the red line represents the October time series. The dotted lines show the linear trends from 2001 to 2023, corresponding to the annual mean (black), September (blue), and October (red).

185

Table 3 summarizes the trends from four datasets along with MLR correlation coefficients (R^2). Antarctic ozone declined steadily at an annual decline rate of 2-3 DU/yr, with a more pronounced rate of 5-6 DU/yr during September and October. The long-term annual trend from 2001 to 2019 was approximately 0.5 DU/yr across multiple datasets, whereas the TOMCAT simulation for 2001- 2023 showed a negative trend (0.4 DU/yr). After 2000, September consistently exhibits positive trends, while October trends shift from weakly positive (0.3 ± 3.2 DU yr⁻¹ for 2001–2019) to significantly negative (-1.5 ± 2.4 DU yr⁻¹ for 2001–2023). This divergence suggests that dynamical processes drive chemical depletion in October, and EESC might not accurately reflect the ozone changes in October.

190



195 Table 3. Linear trends (DU/yr) of TCO in the annual mean, September, and October means with different time spans for each dataset, and the correlation between dataset and MLR (R^2).

		Dataset	TOMCAT	WOUDC	MSR-2	TOMS/OMI
	Time span					
Annual	1979-2000		-3.2 (0.7)	-2.3 (0.4)	-1.9 (0.5)	
	2001-2019		0.5 (1.1)	0.3 (0.6)	0.4 (0.9)	0.3 (1.1)
	2001-2023		-0.4 (0.9)	-0.03 (0.5)	-0.3 (0.7)	-0.2 (0.8)
	R^2		0.85	0.86	0.73	0.67
September	1979-2000		-5.9 (1)	-5 (1.1)	-4.7 (0.8)	
	2001-2019		1.4 (2.4)	1.5 (1.8)	1.5 (2.3)	0.6 (2.8)
	2001-2023		0.1 (1.8)	0.9 (1.3)	0.1 (1.7)	-0.4 (2)
	R^2		0.91	0.88	0.85	0.8
October	1979-2000		-6 (1.9)	-5.4 (1.5)	-5.1 (1.7)	
	2001-2019		0.3 (3.2)	-0.03 (2.4)	0.2 (3)	0.7 (3.1)
	2001-2023		-1.5 (2.4)	-0.8 (1.7)	-1.3 (2.2)	-1 (2.3)
	R^2		0.83	0.77	0.82	0.76

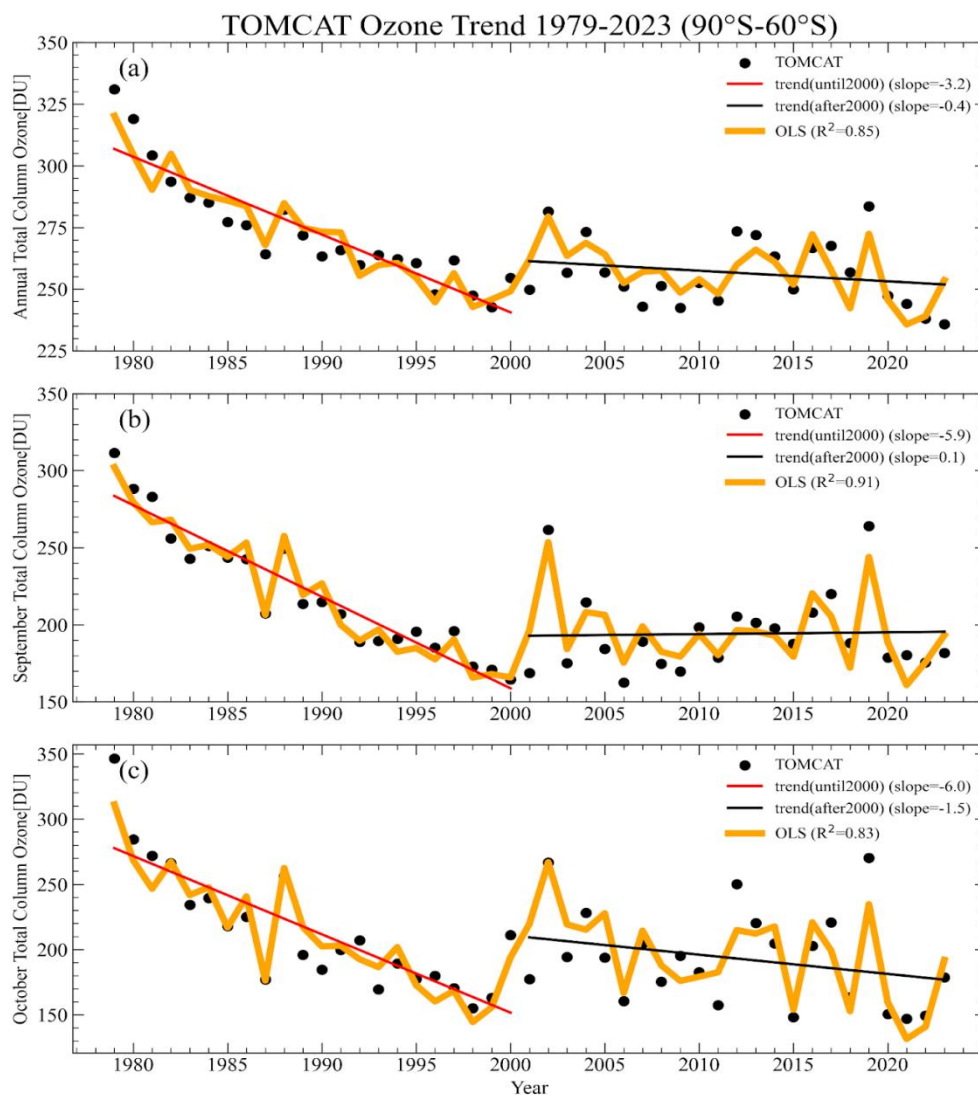


Figure 3. TCO time series of the TOMCAT dataset from 1979 to 2023. (a) Annual mean, (b) September, and (c) October.
200 The black dots are TOMCAT, the orange thick line is time series based on MLR results, the red line is the linear trend of the TOMCAT from 1979 to 2000, and the black is the linear trend of the TOMCAT from 2001 to 2023.

To further evaluate the ability of the regression framework to reproduce observed variability, we examine the TOMCAT-based MLR results in detail. Fig. 3 presents the time series of TCO and the MLR based on the TOMCAT dataset. The results
205 suggest a post-2000 decline, with an interannual trend of -0.4 (0.9) DU/yr and a stronger October trend of -1.5 (2.4) DU/yr. However, September shows a weak positive trend of 0.1 (1.8) DU/yr. Regression analysis across four datasets demonstrates good agreement in the long-term ozone changes. The long-term ozone changes in the MLR can explaining about 85 % of the



variance in the interannual time series. Among them, the MLR of TOMCAT is the largest, explaining 91 % of the variance in the time series, indicating strong reproduction of observed long-term ozone variability.

210

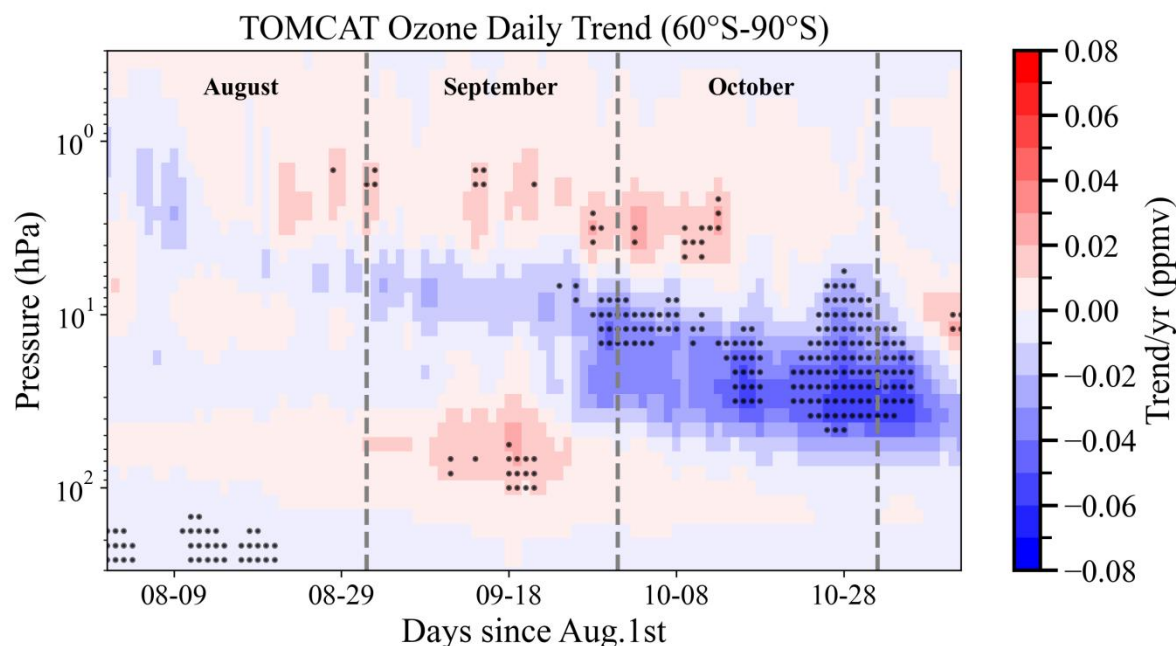


Figure 4. Vertical cross section of daily trends (2001-2023) in ozone volume mixing ratios from TOMCAT. Trends are shown for August 1 to November 10 (2001-2023). Stippled areas are statistically significant above the 95% confidence level.

215 To determine whether the September–October contrast arises from changes at specific altitudes, we examined vertical ozone trends in the austral winter/spring. Ozone mixing ratios from the TOMCAT dataset were analysed as a function of altitude and day of the year (1 August–10 November) for 2001-2023 (Fig. 4). In August, the ozone mixing ratio trend at 1 hPa showed a negative change and gradually extended downward. By September, this trend reached the mid-stratosphere, resulting in a negative anomaly, with a rate of change in the ozone mixing ratio of -0.03 parts per million per year (ppmv/year). However, positive trends dominate the middle and lower stratosphere, reaching ~0.04 ppmv/year, exceeding the magnitude of the negative changes and consistent with the recovery observed in September. In October, a broader negative region emerged (5-80 hPa), peaking at -0.07 ppmv/year and coinciding with the main Antarctic ozone layer (4-20 hPa). The persistent negative trend in ozone continued into early November, suggesting prolonged low Antarctic ozone values and requiring continued monitoring of dynamical and chemical processes driving these trend changes.

225

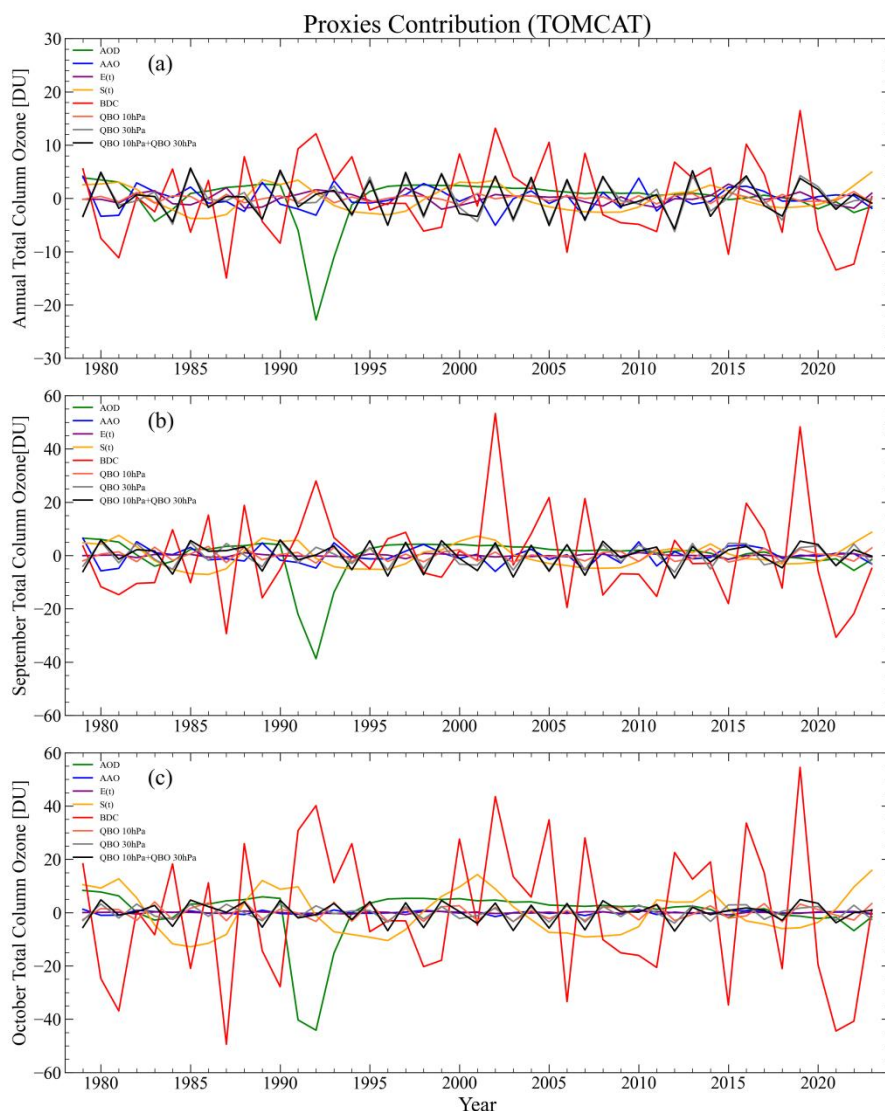


Figure 5. The contribution of each proxy to TCO from 1979 to 2023 based on TOMCAT data. (a) Annual mean, (b) September, and (c) October. Green line: AOD, blue line: AAO, purple line: ENSO, orange line: Solar cycle, red line: BDC, light red line: QBO 10 hPa, grey line: QBO 30 hPa, black line: Overall combined QBO.

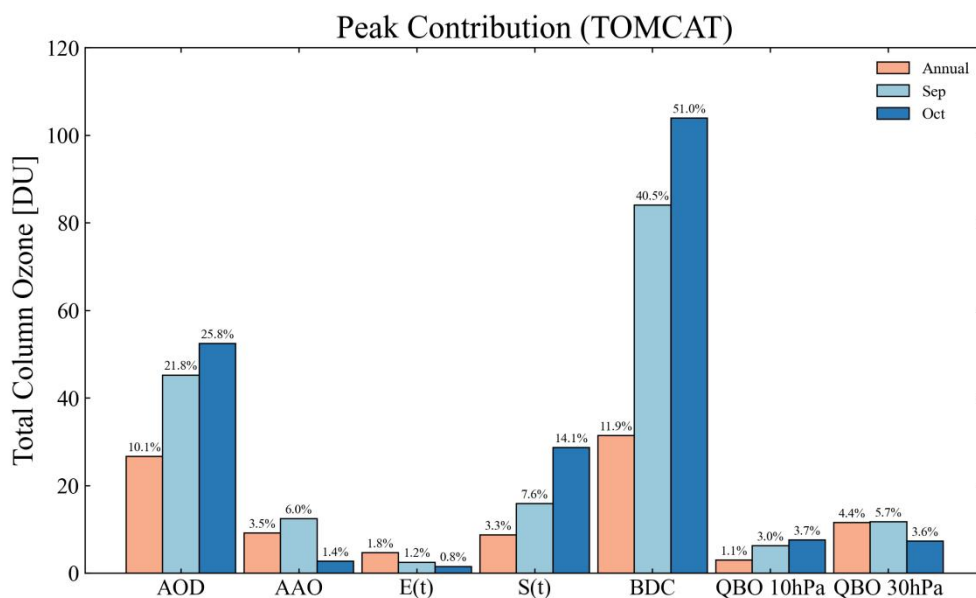
230

To elucidate the impact of each proxy, we analyse their contributions to ozone variation using the MLR results of the TOMCAT dataset. BDC has a significant impact on the long-term ozone variation and recent interannual ozone variability, contributing up to -12 DU during 2020-2023 (Fig. 5a). AOD exerted a significant influence on Antarctic ozone following the El Chichón (1982) and Pinatubo (1991) volcanic eruptions, with a peak contribution of ~ 25 DU. Other proxies contribute less than 6 DU but their influences are not negligible.

235



During the austral winter/spring, the MLR well described the contribution of dynamic processes to stratospheric ozone, with BDC being the main driver of long-term ozone changes. Variations in planetary wave forcing, represented by EHF, modulate the BDC and influence polar vortex behavior. Concurrently, as a factor with periodic fluctuations, solar cycle contributes less than ± 15 DU to ozone variability in September and October (Figs. 5b-c). After a volcanic eruption, AOD will remain high in the stratosphere for a limited period. For instance, the Pinatubo eruption resulted in the largest reduction of up to -40 DU for a few years, and smaller volcanic eruptions, such as the 2022 Hunga Tonga-Hunga Ha'apai volcano eruption in 2022, influenced ozone by up to -7 DU.



245 Figure 6. Peak contribution (unit: DU) of each proxy to TCO changes from 1979 to 2023 based on TOMCAT. Orange: Annual mean; light blue: September; blue: October. The rate of ozone change in percent is labelled above each bar.

Fig. 6 illustrates the peak influence of each proxy on the TCO changes. BDC and AOD dominate interannual variation of ozone, while the combined QBO accounts for up to 5.5% of the variance. The dominant role of BDC can be explained by its transport of ozone from the tropics to high latitudes, with ozone accumulation reaching a maximum at mid to high latitudes from May to September. During winter, ozone is transported from mid latitudes to the polar regions in spring, and the efficiency of this transport depends on the strength of BDC (Weber et al., 2011; Fioletov et al., 2023). These transport processes lead to a more pronounced contribution of BDC to the long-term ozone variability in September and October, with



255 peak rate reaching 51%, indicating its significant impact on Antarctica TCO fluctuation. Comparatively, peak contributions of QBO and solar cycle are approximately 8% in September, whereas other proxies contribute less than 6%.

5 Model simulations

5.1 Setup of the model sensitivity experiment

260 Figures 5 and 6 clearly show that variations in BDC strength have a profound impact on the Antarctic ozone recovery. To investigate the role of BDC on Antarctic ozone, we performed two sensitivity simulations using TOMCAT to explore the modulation effect of BDC on ozone. The control experiment (CRL) uses the standard chemical and dynamical parameters spanning the period 2000-2009. To assess the impact of BDC intensity, two sensitivity experiments were conducted based on typical years of BDC anomalies: EXP1 represents a year with strong BDC (2002), while EXP2 represents a year with weak
265 BDC (2006). In these experiments, wind forcing and temperature from 2000 to 2009 was altered to modify BDC intensity, while other parameters remain unchanged. The experimental design is summarized in Table 4.

The selection of 2002 and 2006 as typical years was guided by interannual variation of ozone and ODS changes to ensure that the BDC intensity is the dominant factor influencing the ozone variation. Previous studies have shown a weakening of
270 ozone transport to the polar regions in 2006, accompanied by persistent cold temperatures and stable polar vortex in late winter and early spring (Peshin, 2008; Grytsai, 2011). In contrast, the typical strengthening of BDC occurred in 2002 as a result of unusually strong upward planetary wave propagation. Elevated stratospheric temperature in the SH, along with polar vortex splitting, created an unfavorable environment for polar ozone depletion (Allen et al., 2003; Sinnhuber et al., 2003). These marked differences in circulation intensity highlight the contrasting dynamical regimes of 2002 and 2006,
275 making them ideal case studies for examining the role of BDC in Antarctic ozone variability.

Table 4. Experimental design.

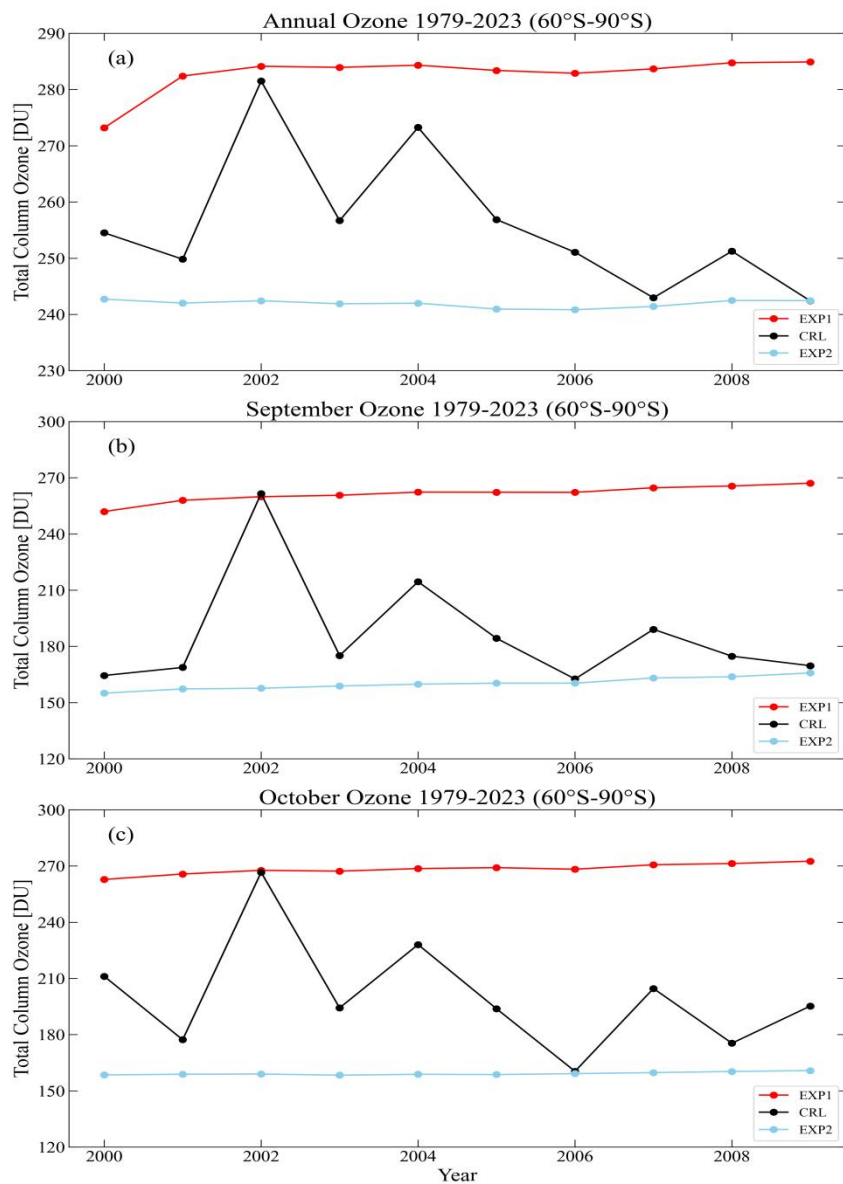
Trial	Simulation Result	Simulation Process
Control experiment (CRL)	TOMCAT Dataset for 2000-2009	-



Sensitivity experiment 1 (EXP1)	Simulated TOMCAT dataset for 2000-2009	The 2002 wind forcing and temperatures are applied to all years during 2000-2009 and other variables are unchanged from the CRL.
Sensitivity experiment 2 (EXP2)	Simulated TOMCAT dataset for 2000-2009	Same as EXP1, but wind forcing and temperatures of 2006 applied for all years.

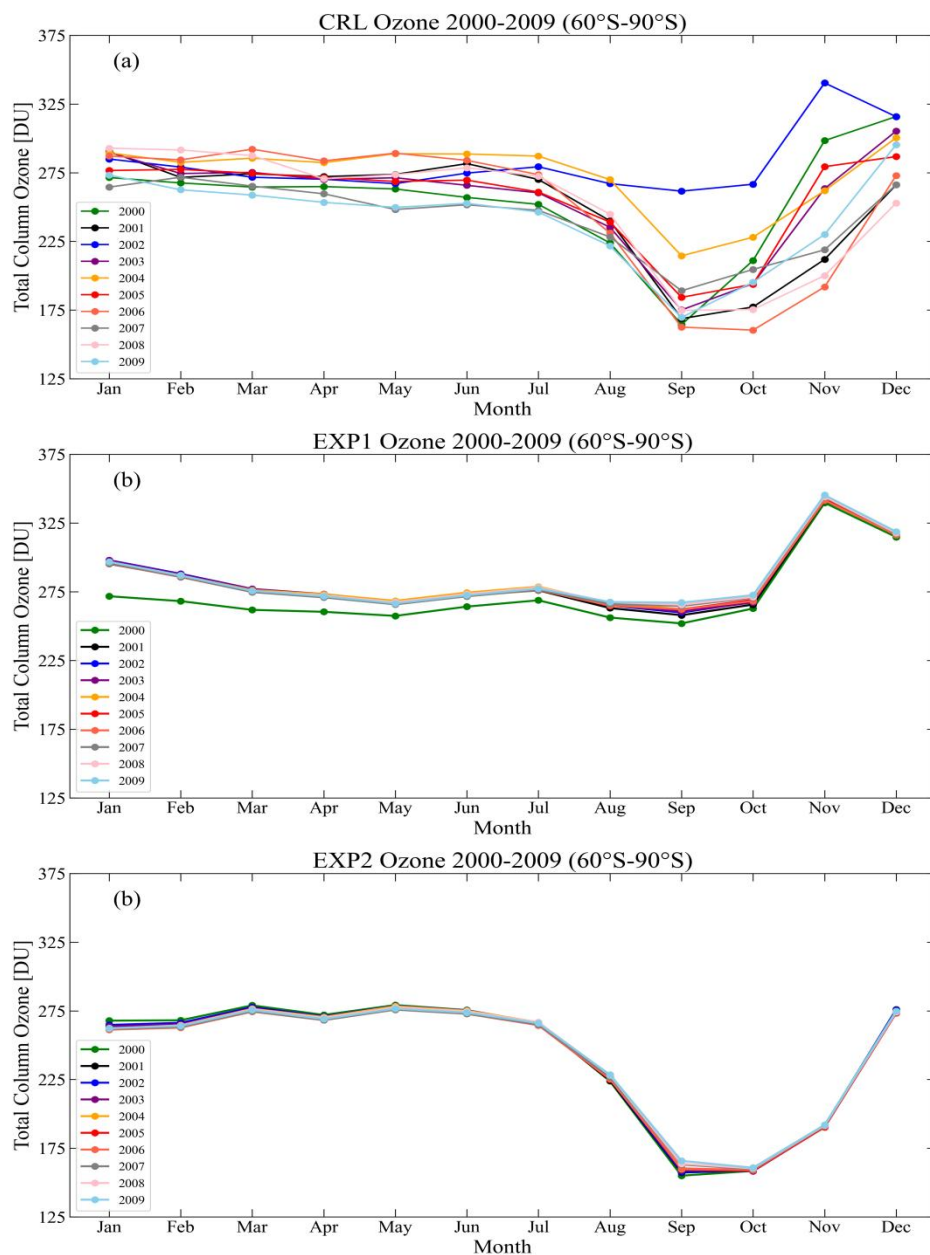
5.2 Simulation result

280 An increase in TCO is observed in EXP1 (strong BDC; Fig. 7), with values from 2000 to 2009 approximating those in 2002. Conversely, EXP2 (weak BDC) reveals ozone reductions, with September and October ozone values resembling those in 2006. The sensitivity experiment results suggest that the peak contribution rates are consistent with the MLR results, with the annual mean and October peak contribution rates of ~15% and ~52%, respectively.



285

Figure 7. TCO changes in Antarctica for control and sensitivity experiments from 2000-2009. (a) Annual mean, (b) September, and (c) October. Red: EXP1 (weak BDC), sky blue: EXP2 (strong BDC), black: CRL.

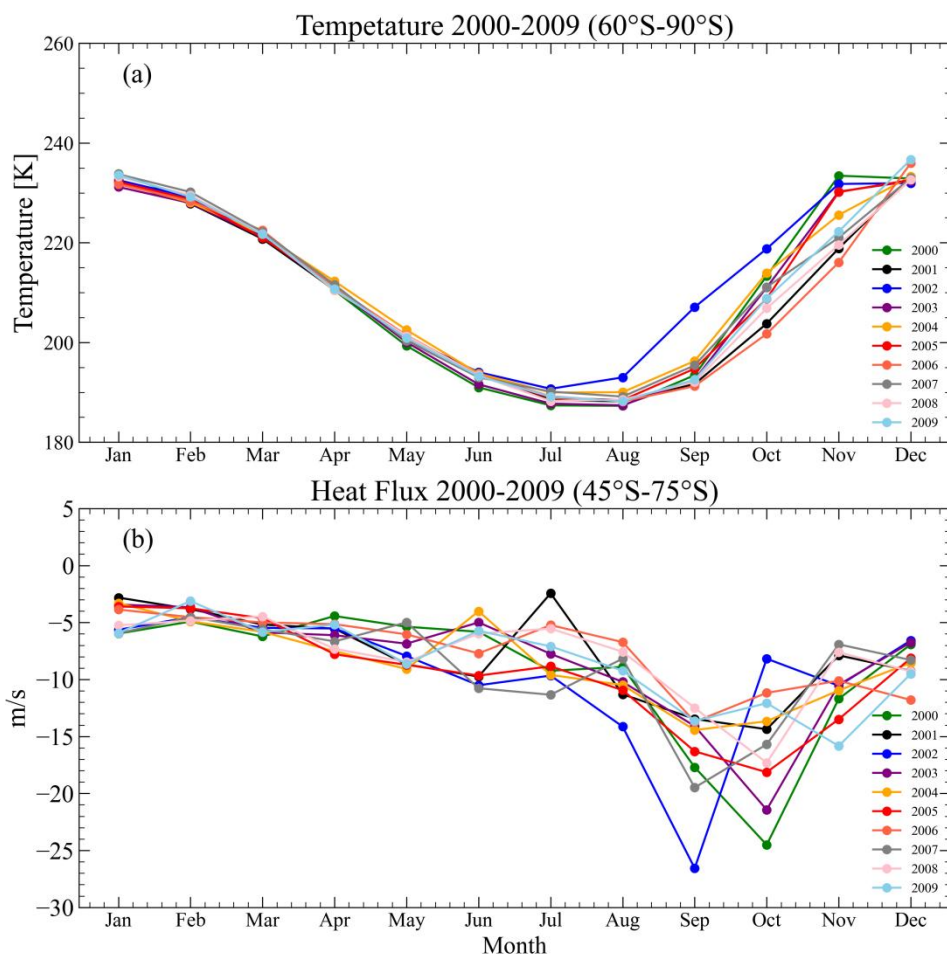


290 Figure 8. Monthly TCO in the Antarctic for control and sensitivity experiments. (a) CRL, (b) EXP1, and (c) EXP2.

Monthly TCO changes for control and sensitivity experiments from 2000 to 2009 are illustrated in Figure 8. Ozone typically experiences pronounced depletion in September, with TCO dropping below 220 DU, a threshold associated with the formation of the ozone hole. In 2002, September and October showed significant anomalies, with TCO values reaching 250
295 DU. According to the EXP1, enhanced circulation during the winter and spring increased TCO towards those of 2002. In



contrast, during spring of 2006, the lowest TCO of the decade occurred, with a substantial ozone hole persisting into October (TCO ~ 150 DU). Recovery signs emerged in November, delayed by persistent low temperatures and the protracted breakup of the polar vortex.



300

Figure 9. (a) Monthly mean temperature at 50 hPa in Antarctica. (b) Monthly mean eddy heat flux (EHF) at 100 hPa (45° S-75° S).

Figure 9a shows the monthly mean temperature at 50 hPa from 2000 to 2009. The abnormal increase in temperature in the winter and spring of 2002 coincided with higher TCO, while the cooler temperatures in the spring of 2006 were associated with the persistently low ozone values (Fig. 8 and Fig. 9a). These temperature variations are inextricably linked to BDC strength and the timing of vortex breakup (Weber et al., 2011; Butchart, 2014). As shown in Fig. 9b, EHF was high in the spring and winter of 2006, indicating the weakened circulation and reduced ozone transport from the tropics to the polar

305

regions. Meanwhile, the persistent stratosphere cooling favored vortex survival and delayed breakup, resulting in a
310 prolonged and extensive ozone hole in 2006.

The mechanistic link between circulation and ozone is clear. In 2002, enhanced planetary wave activity strengthened the
BDC, promoting tropical-to-polar ozone transport. Elevated temperatures have suppressed the efficiency of stratospheric
cloud formation, limiting ozone depletion. The polar vortex split over Antarctica, with one part moving equatorward in the
315 South Pacific and the other remaining over Antarctica, but the anomalies triggered an earlier breakup than in previous years.
The combination of strong BDC transport, favorable temperatures and split vortex dynamics led to exceptionally high TCO
in 2002, primarily related to the SSW and enhanced transport mechanisms (Sinnhuber et al., 2003; Wang et al., 2005).

6 Summary and conclusions

320 This study combined satellite-based observations, reanalysis datasets as well as chemistry-climate model simulations to
analyze the latest long term ozone trend over Antarctica during 1979-2023. Using MLR, we analyzed the contributions of
dynamical and chemical proxies to ozone variability. Based on the TOMCAT 3-D model, we conducted sensitivity
experiments to investigate the impact of the BDC on ozone. Important conclusions are:

(1) Multiple datasets can consistently well represent the long-term ozone changes over Antarctica. In 2001-2019, annual
325 ozone showed signs of recovery, while the annual change in TCO shifted downward at -0.4 (1.1) DU/yr during 2001-2023.

(2) The MLR reproduces observed long-term ozone changes with high fidelity, explaining about 67-91 % of the variance in
the time series over the Antarctic. The daily ozone trends based on TOMCAT dataset during the period 2001-2023 showed
that the recovery of ozone in September is due to increasing ozone trends in the lowermost stratosphere. While in October,
negative trends are observed in the entire lower stratosphere. This seasonal contrast explains why the TCO trends are
330 negative in October but slightly positive in September.

(3) Proxy analysis highlights the dominant role of BDC in the Antarctic spring, with volcanic aerosol forcing, particularly
following the Pinatubo eruption, producing substantial ozone losses. Other proxies also exert smaller but non-negligible
contributions to the ozone change.

(4) Sensitivity experiments further reveal that the strengthening (weakening) of BDC led to an increase (decrease) in the
335 transport of tropical ozone to polar regions. The BDC anomaly in the SH significantly affects the polar temperature, and
thereby ozone depletion, with circulation anomalies capable of driving large monthly variability as high as 51% in October.

Overall, in the long-term, Antarctic ozone evolution reflects the interplay of multiple processes, with dynamical drivers
holding a particularly strong influence on recovery patterns. BDC perturbations play a significant role in the long-term ozone
trend, requiring more research and continued attention to the ozone hole and dynamic processes to improve our
340 understanding of long-term ozone variability and predict future changes in the Antarctic ozone hole.



Data availability

Observational and satellite data used are available in Sect. 2. The TOMCAT/SLIMCAT model data used is supported by the University of Leeds.

Author contributions

345 HH analysed the data and prepared the manuscript under the guidance of SC. MPC, SSD, WF, SC, YL, MW, SH supported the discussion, interpretation and analyse, and helped to write the paper. MPC provided support in model running and processing. All authors edited and contributed to the write of the manuscript.

Competing interests

The authors declare that they have no conflict of interest with other people.

350 **Acknowledgements**

We are grateful to WOUDC, NASA, and NOAA for providing global ozone datasets. We are grateful to all the providers of meteorological data used in this study. MC, SD, and MW are grateful for the partial support from the ESA OREGANO Contract 4000137112/22/I-AG ("Ozone Recovery from Merged Observational Data and Model Analysis"). SH was supported by the Leeds-York-Hull Natural Environment Research Council (NERC) Doctoral Training Partnership (DTP) 355 Panorama under grant NE/S007458/1.

Financial support

This research was funded by National Natural Science Foundation of China (42475082 and 4272406), Tropical Ocean Environment in Western Coastal Waters Observation and Research Station of Guangdong Province (2024B1212040008), 360 Innovative Team Plan for Department of Education of Guangdong Province (No. 2023KCXTD015), First-Class Discipline Plan of Guangdong Province (080503032101 and 231420003), Innovation Team Project of General University in Guangdong Province of China (No. 2024KCXTD042) and the Jiangsu Province Natural Science Foundation Youth Fund Project (BK20230115).



References

- 365 Allen, D. R., Bevilacqua, R. M., Nedoluha, G. E., Randall, C. E., and Manney, G. L.: Unusual stratospheric transport and mixing during the 2002 Antarctic winter, *Geophys. Res. Lett.*, 30, <https://doi.org/10.1029/2003gl017117>, 2003.
- Aquila, V., Oman, L. D., Stolarski, R., Douglass, A. R., and Newman, P. A.: The Response of Ozone and Nitrogen Dioxide to the Eruption of Mt. Pinatubo at Southern and Northern Midlatitudes, *J. Atmos. Sci.*, 70, 894-900, <https://doi.org/10.1175/jas-d-12-0143.1>, 2013.
- 370 Ball, W. T., Alsing, J., Staehelin, J., Davis, S. M., Froidevaux, L., and Peter, T.: Stratospheric ozone trends for 1985–2018: sensitivity to recent large variability, *Atmos. Chem. Phys.*, 19, 12731-12748, <https://doi.org/10.5194/acp-19-12731-2019>, 2019.
- Ball, W. T., Alsing, J., Mortlock, D. J., Staehelin, J., Haigh, J. D., Peter, T., Tummon, F., Stübi, R., Stenke, A., and Anderson, J.: Evidence for a continuous decline in lower stratospheric ozone offsetting ozone layer recovery, *Atmos. Chem. Phys.*, 18, 1379-1394, <https://doi.org/10.5194/acp-18-1379-2018>, 2018.
- 375 Butchart, N.: The Brewer-Dobson circulation, *Rev. Geophys.*, 52, 157-184, <https://doi.org/10.1002/2013rg000448>, 2014.
- Camp, C. D. and Tung, K. K.: Stratospheric polar warming by ENSO in winter: A statistical study, *Geophys. Res. Lett.*, 34, e2006gl028521, <https://doi.org/10.1029/2006gl028521>, 2007.
- Chehade, W., Weber, M., and Burrows, J. P.: Total ozone trends and variability during 1979–2012 from merged data sets of various satellites, *Atmos. Chem. Phys.*, 14, 7059–7074, <https://doi.org/10.5194/acp-14-7059-2014>, 2014.
- 380 Chiou, E. W., Bhartia, P. K., McPeters, R. D., Loyola, D. G., Coldewey-Egbers, M., Fioletov, V. E., Van Roozendaal, M., Spurr, R., Lerot, C., and Frith, S. M.: Comparison of profile total ozone from SBUV (v8.6) with GOME-type and ground-based total ozone for a 16-year period (1996 to 2011), *Atmos. Meas. Tech.*, 7, 1681-1692, <https://doi.org/10.5194/amt-7-1681-2014>, 2014.
- 385 Chipperfield, M. P.: New version of the TOMCAT/SLIMCAT off-line chemical transport model: Intercomparison of stratospheric tracer experiments, *Q. J. R. Meteorolog. Soc.*, 132, 1179–1203, <https://doi.org/10.1256/qj.05.51>, 2006.
- Chipperfield, M. P., Bekki, S., Dhomse, S., Harris, N. R. P., Hassler, B., Hossaini, R., Steinbrecht, W., Thieblemont, R., and Weber, M.: Detecting recovery of the stratospheric ozone layer, *Nature*, 549, 211-218, <https://doi.org/10.1038/nature23681>, 2017.
- 390 Chipperfield, M. P., Dhomse, S., Hossaini, R., Feng, W., Santee, M. L., Weber, M., Burrows, J. P., Wild, J. D., Loyola, D., and Coldewey-Egbers, M.: On the Cause of Recent Variations in Lower Stratospheric Ozone, *Geophys. Res. Lett.*, 45, 5718-5726, <https://doi.org/10.1029/2018gl078071>, 2018.
- Coddington, O., Lean, J. L., Pilewskie, P., Snow, M., and Lindholm, D.: A Solar Irradiance Climate Data Record, *Bull. Am. Meteorol. Soc.*, 97, 1265-1282, <https://doi.org/10.1175/bams-d-14-00265.1>, 2016.



- 395 Dhomse, S., Kinnison, D., Chipperfield, M. P., Cionni, I., Hegglin, M., Abraham, N. L., Akiyoshi, H., Archibald, A. T.,
Bednarz, E. M., and Bekki, S.: Estimates of ozone return dates from Chemistry-Climate Model Initiative simulations, *Atmos.*
Chem. Phys. Discuss., 2018, 1-40, <https://doi.org/10.5194/acp-18-8409-2018>, 2018.
- Dhomse, S. S., Weber, M., Wohltmann, I., Rex, M., and Burrows, J. P.: On the possible causes of recent increases in
northern hemispheric total ozone from a statistical analysis of satellite data from 1979 to 2003, *Atmos. Chem. Phys.*, 6,
400 1165-1180, <https://doi.org/10.5194/acp-6-1165-2006>, 2006.
- Dhomse, S. S., Chipperfield, M. P., Feng, W., Hossaini, R., Mann, G. W., and Santee, M. L.: Revisiting the hemispheric
asymmetry in midlatitude ozone changes following the Mount Pinatubo eruption: A 3-D model study, *Geophys. Res. Lett.*,
42, 3038-3047, <https://doi.org/10.1002/2015GL063052>, 2015.
- Dhomse, S. S., Chipperfield, M. P., Feng, W., Hossaini, R., Mann, G. W., Santee, M. L., and Weber, M.: A single-peak-
405 structured solar cycle signal in stratospheric ozone based on Microwave Limb Sounder observations and model simulations,
Atmos. Chem. Phys., 22, 903-916, <https://doi.org/10.5194/acp-22-903-2022>, 2022.
- Dhomse, S. S., Chipperfield, M. P., Damadeo, R. P., Zawodny, J. M., Ball, W. T., Feng, W., Hossaini, R., Mann, G. W., and
Haigh, J. D.: On the ambiguous nature of the 11 year solar cycle signal in upper stratospheric ozone, *Geophys. Res. Lett.*, 43,
7241-7249, <https://doi.org/10.1175/10.1002/2016gl069958>, 2016.
- 410 Farman, J. C., Gardiner, B. G., and Shanklin, J. D.: Large losses of total ozone in Antarctica reveal seasonal ClO x/NO x
interaction, *Nature*, 315, 207-210, <https://doi.org/10.1038/315207a0>, 1985.
- Fioletov, V., Zhao, X., Abboud, I., Brohart, M., Ogyu, A., Sit, R., Lee, S. C., Petropavlovskikh, I., Miyagawa, K., Johnson,
B. J., Cullis, P., Booth, J., McConville, G., and McElroy, C. T.: Total ozone variability and trends over the South Pole during
the wintertime, *Atmos. Chem. Phys.*, 23, 12731-12751, <https://doi.org/10.5194/acp-23-12731-2023>, 2023.
- 415 Fioletov, V. E., Bodeker, G. E., Miller, A. J., McPeters, R. D., and Stolarski, R.: Global and zonal total ozone variations
estimated from ground-based and satellite measurements: 1964–2000, *J. Geophys. Res.: Atmos.*, 107, ACH 21-21-ACH 21-
14, <https://doi.org/10.1029/2001jd001350>, 2002.
- Godin-Beekmann, S., Azouz, N., Sofieva, V. F., Hubert, D., Petropavlovskikh, I., Effertz, P., Ancellet, G., Degenstein, D. A.,
Zawada, D., Froidevaux, L., Frith, S., Wild, J., Davis, S., Steinbrecht, W., Leblanc, T., Querel, R., Tourpali, K., Damadeo,
420 R., Maillard Barras, E., Stübi, R., Vigouroux, C., Arosio, C., Nedoluha, G., Boyd, I., Van Malderen, R., Mahieu, E., Smale,
D., and Sussmann, R.: Updated trends of the stratospheric ozone vertical distribution in the 60° S–60° N latitude range based
on the LOTUS regression model, *Atmos. Chem. Phys.*, 22, 11657-11673, <https://doi.org/10.5194/acp-22-11657-2022>, 2022.
- Gray, L. J., Beer, J., Geller, M., Haigh, J. D., Lockwood, M., Matthes, K., Cubasch, U., Fleitmann, D., Harrison, G., and
Hood, L.: Solar influences on climate, *Rev. Geophys.*, 48, <https://doi.org/10.1029/2009RG000282>, 2010.
- 425 Grytsai, A.: Planetary wave peculiarities in Antarctic ozone distribution during 1979–2008, *Int. J. Remote Sens.*, 32, 3139-
3151, <https://doi.org/10.1080/01431161.2010.541518>, 2011.
- Harris, N. R. P., Kyrö, E., Staehelin, J., Brunner, D., Andersen, S.-B., Godin-Beekmann, S., Dhomse, S., Hadjinicolaou, P.,
Hansen, I. I., G. , Jrrar, A., Karpetchko, A., Kivi, B. K., R. , Krizan, P., Lastovicka, J., Maeder, J., Orsolini, Y., A. Pyle, J.,



- Rex, K. V., M., Weber, M., Wohltmann, I., Zanis, P., and Zerefos, C.: Ozone trends at northern mid- and high latitudes – a
430 European perspective, *Ann. Geophys.*, 26, 1207–1220, <https://doi.org/10.5194/angeo-26-1207-2008>, 2008.
- Kessenich, H. E., Seppala, A., and Rodger, C. J.: Potential drivers of the recent large Antarctic ozone holes, *Nat. Commun.*,
14, 7259, <https://doi.org/10.1038/s41467-023-42637-0>, 2023.
- Khaykin, S., Legras, B., Bucci, S., Sellitto, P., Isaksen, L., Tencé, F., Bekki, S., Bourassa, A., Rieger, L., Zawada, D.,
435 Jumelet, J., and Godin-Beekmann, S.: The 2019/20 Australian wildfires generated a persistent smoke-charged vortex rising
up to 35 km altitude, *Commun. Earth Environ.*, 1, 22, <https://doi.org/10.1038/s43247-020-00022-5>, 2020.
- Knepp, T. N., Kovilakam, M., Thomason, L., and Miller, S. J.: Characterization of stratospheric particle size distribution
uncertainties using SAGE II and SAGE III/ISS extinction spectra, *Atmos. Meas. Tech.*, 17, 2025–2054,
<https://doi.org/10.5194/amt-17-2025-2024>, 2024.
- Levelt, P. F., Van Den Oord, G. H., Dobber, M. R., Malkki, A., Visser, H., De Vries, J., Stammes, P., Lundell, J. O., and
440 Saari, H.: The ozone monitoring instrument, *IEEE Trans. Geosci. Remote Sens.*, 44, 1093–1101,
<https://doi.org/10.1109/TGRS.2006.872333>, 2006.
- Levelt, P. F., Joiner, J., Tamminen, J., Veefkind, J. P., Bhartia, P. K., Stein Zweers, D. C., Duncan, B. N., Streets, D. G.,
Eskes, H., and van der A, R.: The Ozone Monitoring Instrument: overview of 14 years in space, *Atmos. Chem. Phys.*, 18,
5699–5745, <https://doi.org/10.5194/acp-18-5699-2018>, 2018.
- 445 Li, Y., Chipperfield, M. P., Feng, W., Dhomse, S. S., Pope, R. J., Li, F., and Guo, D.: Analysis and attribution of total
column ozone changes over the Tibetan Plateau during 1979–2017, *Atmos. Chem. Phys.*, 20, 8627–8639,
<https://doi.org/10.5194/acp-20-8627-2020>, 2020.
- Li, Y., Dhomse, S. S., Chipperfield, M. P., Feng, W., Bian, J., Xia, Y., and Guo, D.: Quantifying stratospheric ozone trends
over 1984–2020: a comparison of ordinary and regularized multivariate regression models, *Atmos. Chem. Phys.*, 23, 13029–
450 13047, <https://doi.org/10.5194/acp-23-13029-2023>, 2023.
- Nair, P. J., Godin-Beekmann, S., Kuttippurath, J., Ancellet, G., Goutail, F., Pazmiño, A., Froidevaux, L., Zawodny, J. M.,
Evans, R. D., Wang, H. J., Anderson, J., and Pastel, M.: Ozone trends derived from the total column and vertical profiles at a
northern mid-latitude station, *Atmos. Chem. Phys.*, 13, 10373–10384, <https://doi.org/10.5194/acp-13-10373-2013>, 2013.
- Newman, P. A., Nash, E. R., and Rosenfield, J. E.: What controls the temperature of the Arctic stratosphere during the
455 spring?, *J. Geophys. Res.: Atmos.*, 106, 19999–20010, <https://doi.org/10.1029/2000JD000061>, 2001.
- Newman, P. A., Daniel, J. S., Waugh, D. W., and Nash, E. R.: A new formulation of equivalent effective stratospheric
chlorine (EESC), *Atmos. Chem. Phys.*, 7, 4537–4552, <https://doi.org/10.5194/acp-7-4537-2007>, 2007.
- Newman, P. A., Nash, E. R., Kawa, S. R., Montzka, S. A., and Schauffler, S. M.: When will the Antarctic ozone hole
recover?, *Geophys. Res. Lett.*, 33, <https://doi.org/10.1029/2005gl025232>, 2006.
- 460 Peshin, S. K.: Depletion of ozone over Antarctica during 2006, *MAUSAM*, 59, 313–320,
<https://doi.org/10.54302/mausam.v59i3.1262>, 2008.



- Peterson, D. A., Fromm, M. D., McRae, R. H. D., Campbell, J. R., Hyer, E. J., Taha, G., Camacho, C. P., Kablick, G. P., Schmidt, C. C., and DeLand, M. T.: Australia's Black Summer pyrocumulonimbus super outbreak reveals potential for increasingly extreme stratospheric smoke events, *npj Clim. Atmos. Sci.*, 4, <https://doi.org/10.1038/s41612-021-00192-9>, 2021.
- 465 Ramanathan, V., Cicerone, R. J., Singh, H. B., and Kiehl, J. T.: Trace gas trends and their potential role in climate change, *J. Geophys. Res.: Atmos.*, 90, 5547-5566, <https://doi.org/10.1029/JD090iD03p05547>, 1985.
- Randel, W. J., Wu, F., and Stolarski, R.: Changes in Column Ozone Correlated with the Stratospheric EP Flux, *J. Meteorolog. Soc. Jpn.*, 80, 849-862, <https://doi.org/10.2151/jmsj.80.849>, 2002.
- 470 Sato, M., E. Hansen, J., McCormick, M. P., and B. Pollack, J.: Stratospheric aerosol optical depths, 1850-1990, *J. Geophys. Res.: Atmos.*, 98, 22987-22994, <https://doi.org/10.1029/93jd02553>, 1993.
- Sinnhuber, B. M., Weber, M., Amankwah, A., and Burrows, J. P.: Total ozone during the unusual Antarctic winter of 2002, *Geophys. Res. Lett.*, 30, 1580, <https://doi.org/10.1029/2002gl016798>, 2003.
- Snow, M., Weber, M., Machol, J., Viereck, R., and Richard, E.: Comparison of Magnesium II core-to-wing ratio observations during solar minimum 23/24, *J. Space Weather Space Clim.*, 4, A04, <https://doi.org/10.1051/swsc/2014001>, 2014.
- 475 Solomon, S., Rolando, R. G., F. Sherwood, R., and Donald, J. W.: On the depletion of Antarctic ozone, *Nature*, 321, 755-758, <https://doi.org/10.1038/321755a0>, 1986.
- Steinbrecht, W., Froidevaux, L., Fuller, R., Wang, R., Anderson, J., Roth, C., Bourassa, A., Degenstein, D., Damadeo, R., and Zawodny, J.: An update on ozone profile trends for the period 2000 to 2016, *Atmos. Chem. Phys.*, 17, 10675-10690, <https://doi.org/10.5194/acp-17-10675-2017>, 2017.
- Thompson, D. W. and Solomon, S.: Interpretation of recent Southern Hemisphere climate change, *Science*, 296, 895-899, <https://doi.org/10.1126/science.1069270>, 2002.
- Van Der A, R. J., Allaart, M. A. F., and Eskes, H. J.: Multi sensor reanalysis of total ozone, *Atmos. Chem. Phys.*, 10, 11277-11294, <https://doi.org/10.5194/acp-10-11277-2010>, 2010.
- 485 Velders, G. J., Andersen, S. O., Daniel, J. S., Fahey, D. W., and McFarland, M.: The importance of the Montreal Protocol in protecting climate, *Proceedings of the National Academy of Sciences*, 104, 4814-4819, <https://doi.org/10.1073/pnas.0610328104>, 2007.
- Wang, D. Y., von Clarmann, T., Fischer, H., Funke, B., García-Comas, M., Gil-López, S., Glatthor, N., Grabowski, U., Höpfner, M., Kellmann, S., Kiefer, M., Koukouli, M. E., Lin, G., Linden, A., López-Puertas, M., Mengistu Tsidu, G., Milz, M., Steck, T., and Stiller, G. P.: Longitudinal variations of temperature and ozone profiles observed by MIPAS during the Antarctic stratosphere sudden warming of 2002, *J. Geophys. Res.: Atmos.*, 110, <https://doi.org/10.1029/2004jd005749>, 2005.
- Wargan, K., Orbe, C., Pawson, S., Ziemke, J. R., Oman, L. D., Olsen, M. A., Coy, L., and Emma Knowland, K.: Recent decline in extratropical lower stratospheric ozone attributed to circulation changes, *Geophys. Res. Lett.*, 45, 5166-5176, <https://doi.org/10.1029/2018GL077406>, 2018.
- 495



- Weber, M. and Coldewey-Egber, M.: Total ozone trends from 1979 to 2016 derived from five merged observational datasets – the emergence into ozone recovery, *Atmos. Chem. Phys.*, 18, 2097–2117, <https://doi.org/10.5194/acp-18-2097-2018>, 2018.
- Weber, M., Dikty, S., Burrows, J. P., Garny, H., Dameris, M., Kubin, A., Abalichin, J., and Langematz, U.: The Brewer-Dobson circulation and total ozone from seasonal to decadal time scales, *Atmos. Chem. Phys.*, 11, 11221-11235, <https://doi.org/10.5194/acp-11-11221-2011>, 2011.
- 500 Weber, M., Arosio, C., Coldewey-Egbers, M., Fioletov, V. E., Frith, S. M., Wild, J. D., Tourpali, K., Burrows, J. P., and Loyola, D.: Global total ozone recovery trends attributed to ozone-depleting substance (ODS) changes derived from five merged ozone datasets, *Atmos. Chem. Phys.*, 22, 6843-6859, <https://doi.org/10.5194/acp-22-6843-2022>, 2022.
- Wellmeyer, C. G., Bhartia, P. K., Taylor, S. L., Qin, W., and Ahn, C.: Version 8 total ozone mapping spectrometer (TOMS) algorithm, *Eur. Comm., Kos, Greece*,
- 505 WMO: Scientific Assessment of Ozone Depletion: 2014, Global Ozone Research and Monitoring Project-Report No. 55, Geneva, Switzerland, 2014.
- WMO: Scientific Assessment of Ozone Depletion: 2018, Global Ozone Research and Monitoring Project-Report No. 58, Geneva, Switzerland, 2018.
- 510 WMO: Scientific Assessment of Ozone Depletion: 2022, Global Ozone Research and Monitoring Project-Report No. 278, Geneva, Switzerland, 2022.
- Zhou, X., Dhomse, S. S., Feng, W., Mann, G., Heddell, S., Pumphrey, H., Kerridge, B. J., Latter, B., Siddans, R., Ventress, L., Querel, R., Smale, P., Asher, E., Hall, E. G., Bekki, S., and Chipperfield, M. P.: Antarctic Vortex Dehydration in 2023 as a Substantial Removal Pathway for Hunga Tonga-Hunga Ha'apai Water Vapor, *Geophys. Res. Lett.*, 51, e2023GL107630, <https://doi.org/10.1029/2023gl107630>, 2024.
- 515